Patterned Turbulence in Liquid Metal Flow: Computational Reconstruction of the Hartmann Experiment

Dmitry Krasnov, André Thess, Thomas Boeck, Yurong Zhao, and Oleg Zikanov

Phys. Rev. Lett. **110**, 084501 — Published 19 February 2013

DOI: 10.1103/PhysRevLett.110.084501

Patterned turbulence in liquid metal flow: Computational reconstruction of the Hartmann experiment

Dmitry Krasnov, André Thess, and Thomas Boeck
Institute of Thermodynamics and Fluid Mechanics,
Ilmenau University of Technology, P.O. Box 100565, 98684 Ilmenau, Germany

Yurong Zhao and Oleg Zikanov
Deptartment of Mechanical Engineering, University of Michigan-Dearborn, 48128-1491 MI, USA

We present results of a numerical analysis of Julius Hartmann's historical experiments on flows of mercury in pipes and ducts under the influence of magnetic fields. The computed critical parameters for the laminar-turbulent transition as well as the friction coefficients are in excellent agreement with Hartmann's data. The simulations provide a first detailed view of the flow structures that are experimentally inaccessible. Novel flow regimes with localized turbulent spots near the side walls parallel to the magnetic field and otherwise laminar flow are discovered. We finally suggest how these predictions can be tested in a transparent fluid using optical flow measurement.

Keywords: Magnetohydrodynamics, Transition to turbulence

75 years ago, Julius Hartmann published two articles [1, 2] on flows of mercury in pipes and ducts under the influence of a uniform transverse magnetic field. In [1], he derived an exact solution for the laminar magnetohydrodynamic (MHD) channel flow that would later be called Hartmann profile and would, with its characteristic electromagnetic boundary layer (the Hartmann layer), become a cornerstone of MHD. Paper [2] described a series of ingenious experiments with flows in pipes and ducts. Today the publication of [1, 2] is widely considered as the advent of liquid metal MHD. Since then, MHD has found a variety of applications ranging from understanding the Earth's magnetic field [3] to electromagnetic flow measurement [4–6] and flow control in materials processing [7]. Other uses, such as liquid metal cooling of fusion reactors [8], are forthcoming.

Given that the Hartmann experiment plays a similar role for laminar-turbulent transition in MHD as the 1883 Reynolds experiment [9] for transition in hydrodynamics (HD), it is rather astonishing that it has not been fully explored using modern numerical analysis. Computations are especially important for MHD, where experiments are conducted with opaque liquid metals and the spatial flow structure cannot be directly observed. The difficulty is illustrated by the inconsistency of experimental data on the transition in tubes, i.e. in pipes and ducts. The only reliable transition criterion available in experiments is the qualitative change in the dependence of pressure drop on flow rate. At strong magnetic fields, the transition is reported at the Reynolds number R based on the Hartmann layer thickness around $R_c \approx 400$ [10]. The critical values in [2] are considerably smaller, $R_c \approx 200$, which has led to concerns about the current understanding of the flow as well as possible imperfections in Hartmann's setup.

This Letter presents our analysis of the transitional states in the Hartmann experiment and, generally, in MHD tubes at moderate Reynolds numbers. Numerical simulations conducted in long domains allow us to reveal the spatial flow structure and discover new regimes. The results explain the apparent inconsistency of the experimental measurements of R_c. We also determine the minimum requirements for accurate numerical modeling of transitional flows.

In MHD tube flows with insulating walls and sufficiently strong transverse magnetic fields $\boldsymbol{B}$, the Lorentz force associated with induced electric currents gives rise to velocity distributions with flat cores and characteristic boundary layers: Hartmann layers near the walls perpendicular to $\boldsymbol{B}$ and Shercliff (duct) or Roberts (pipe) layers near the walls parallel to $\boldsymbol{B}$ [1, 11]. The currents cause Joule dissipation and lead to increased drag when the flow is laminar. In turbulent flows, magnetic damping of fluctuations may reduce the drag.

The MHD tube flows belong to the same class of wall-bounded parallel flows as the HD pipe, duct, channel, Couette, and boundary layer flows, in which the transition is subcritical and caused by essentially nonlinear mechanisms [12]. One should, therefore, speak of a range of flow parameters in which the transition or laminarization occur (e.g., recent experiments [13] in pipe), rather than about a sharp threshold. Previous numerical studies, such as [14, 15], examined the transition following the evolution of finite-amplitude perturbations imposed on a laminar flow. Here, we adopt the same approach as in the Hartmann experiments and perform most of the simulations as laminarization tests at constant flow rate, in which B is increased until the initially turbulent flow becomes laminar.

The non-dimensional governing equations are the Navier-Stokes and induction equation in quasistatic ap-

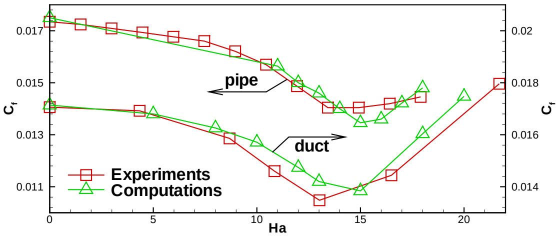

FIG. 1. Friction factor C_f as obtained in our simulations and compared to Hartmann's data recalculated from [2].

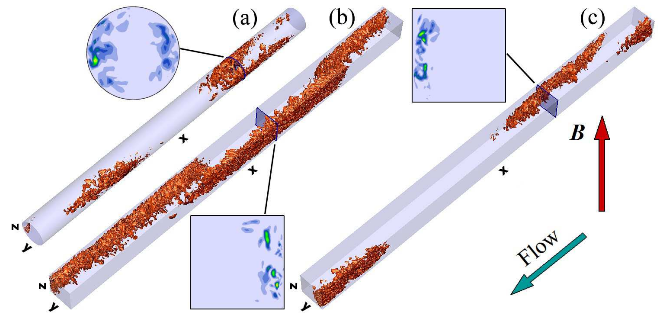

FIG. 2. TKE visualized in the flow domains for: (*a*) pipe at $L_x = 80R$, $Ha = 22$; (*b*) duct at $L_x = 32\pi$, $Ha = 22$; (*c*) duct at $L_x = 32\pi$, $Ha = 25$. Iso-surfaces corresponding to 2% of the maximum are shown. Insets present TKE distributions in selected cross-sections. The isolevels are the same in all insets.

proximation [11]:

$$\frac{\partial \boldsymbol{u}}{\partial t} + (\boldsymbol{u}\cdot\nabla)\boldsymbol{u} = -\nabla p + \frac{1}{Re}\nabla^2\boldsymbol{u} + \frac{Ha^2}{Re}(\boldsymbol{j}\times\boldsymbol{e}_B),$$
$$\nabla\cdot\boldsymbol{u} = 0,\ \boldsymbol{j} = -\nabla\phi + (\boldsymbol{u}\times\boldsymbol{e}_B),\ \nabla^2\phi = \nabla\cdot(\boldsymbol{u}\times\boldsymbol{e}_B),$$

where $\boldsymbol{u}$, p, $\boldsymbol{j}$, ϕ are velocity, pressure, electric current density and potential, and $\boldsymbol{e}_B = \boldsymbol{B}/B$. The nondimensional parameters are the Reynolds and Hartmann numbers $Re \equiv LU/\nu$ and $Ha \equiv BL(\sigma/\rho\nu)^{1/2}$, where σ, ρ, and ν are the fluid electric conductivity, density, and kinematic viscosity, U is the mean velocity, and L is the duct half-width or pipe radius. The conditions at electrically insulating walls are $\boldsymbol{u} = \boldsymbol{0}$ and $\partial\phi/\partial n = 0$. The duct has square cross-section with the magnetic field parallel to one pair of walls.

Computations are performed in domains with periodic inlet/exit boundaries using the conservative, second-order finite-difference scheme described in [16, 17]. The grid is clustered near the walls. For the pipe, the number of grid points N_x(per unit length) $\times N_r \times N_\theta$ is $20\times 64\times 256$. The grid for the duct has N_x(per unit length) $\times N_y \times N_z = 20\times 128\times 128$ points. A comprehensive series of simulations with long domains (up to 64π for duct and 160 for pipe) and run times has been performed. This has been achieved by massive parallelization, with about 300000 CPU-hours consumed in the course of computations (Juropa supercomputer at Forschungszentrum Jülich). Further details of the numerical model and grid sensitivity studies are described in the electronic supplement.

We start with the computations conducted to reproduce two sets of data reported in [2]: the pipe case K12 at $Re = 3500$ and the duct case K27 at $Re = 3000$. The aspect ratio of the duct sides in K27 is 1.12, which is closest to our geometry among the experiments [2] conducted at Re sufficiently high to generate turbulence.

Fig. 1 shows the friction factor $C_f \equiv 2\partial_x PL/\rho U^2$ ($\partial_x P$ is the mean pressure gradient) as a function of Ha. The numerical data are obtained in domains of length of 80 (pipe) and 16π (duct) by averaging over not less than 500 time units. The agreement with the experiments is quite good, with the largest relative discrepancy in C_f being within 3%.

The shape of the curves $C_f(Ha)$ with the characteristic 'dips' can be explained by transformation in response to the magnetic field. Both flows are fully turbulent at $Ha \leq 12$. They become entirely laminar at $Ha \geq 16$ (pipe) or $Ha \geq 15$ (duct). Between the two limits, the flows have the transitional form discussed below. It is known from [18–21] and confirmed by our computations that the suppression of turbulence and reduction of momentum transport by the magnetic field result, in the considered range of Re and Ha, in a decrease of C_f. After the flow becomes laminar, increase of Ha means thinner Hartmann and sidewall layers and, thus, stronger gradient of mean velocity near the walls and higher C_f.

One possible explanation of the small discrepancy between experimental and computational data is the proximity of the starting point for measuring pressure drop to the edge of the magnet ($\sim$ 10 diameters) [2]. This means that the flow evolution after the entrance into the magnet has a non-negligible contribution to the measured pressure drop. Another possible reason for discrepancy in the transitional region will become clear in the following discussion. The intermittent character of the flow requires very large averaging times not easily achievable in computations.

The rest of this Letter explores the transitional states. We use results of extensive simulations of pipe and duct flows at $Re = 5000$. In comparison with the cases in Fig. 1, the principal features of the states remain unchanged, but the range of Ha, where they are detected, is increased. Specifically, in our runs with the longest domains, fully turbulent flows are always found at $Ha \leq 18$ for pipe and $Ha \leq 21$ for duct. Complete laminarization is observed at $Ha \geq 23$ and $Ha \geq 26$, respectively. The typical flow states found between these limits are presented in Fig. 2 using instantaneous low-level isosurfaces of the turbulent kinetic energy (TKE) of transverse velocity $q = u_y^2 + u_z^2$ (duct) or $q = u_r^2 + u_\theta^2$ (pipe). We see the main feature of the transitional regimes – localized

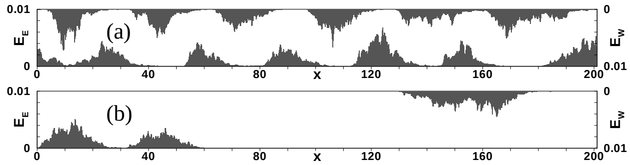

FIG. 3. Two regimes with different puff-patterns in duct at $L_x = 64\pi$, $Ha = 25$. Integrated TKE for east (E_E, lower curves) and west (E_W, upper curves) sides is shown.

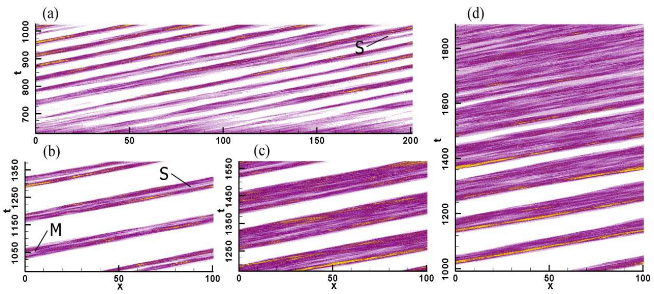

FIG. 4. Evolution of turbulent spots in ducts shown as spatio-temporal distribution of integrated TKE $E(t,x)$: *(a)* E_W at $L_x = 64\pi$, $Ha = 25$ (see Fig. 3a); *(b)* E_E at $L_x = 32\pi$, $Ha = 25$ (see Fig. 2c); *(c)* E_E at $L_x = 32\pi$, $Ha = 22$ (see Fig. 2b); *(d)* E_E in another run at $L_x = 32\pi$, $Ha = 22$. Labels M and S mark the events of puff merging and splitting.

turbulent spots with laminar flow between them.

Localized turbulent spots are well known from HD wall-bounded shear flows [22–27] and can be considered in the broader context of patterned turbulence. The best known example is pipe flow, where the spots are known since [9]. Two types of spots have been identified [22–26]: turbulent puffs with nearly constant length and speed existing in low-Re flows with strong perturbations and turbulent slugs at high Re characterized by aggressive length growth leading to a completely turbulent state. A discussion of their fascinating features, including vorticity dynamics, their nature as a chaotic saddle and the random character and sensitivity to initial conditions, can be found in [22–26].

A major new feature of the turbulent spots in our MHD case is their localization near the sidewalls. As seen in Fig. 2, the flow in the core and the Hartmann layers remains essentially laminar. The phenomenon is observed in all the transitional regimes found in our computations for both the pipe and the duct. We note that, while the turbulent spot pattern is a novel flow regime, turbulent sidewall layers in otherwise laminar flow have been found in ducts at high Re and Ha [17, 28].

We analyze the behavior of the turbulent spots using TKE q. In addition to the $3D$ distributions in Fig. 2, we use TKE integrated over the parts of the cross-section, where the spots are located $E(x,t) = \int_\Omega q d\Omega$. For the duct, Ω is a rectangle of full height and width $1/2$ adjacent to a sidewall. For the pipe, Ω is a ring sector $1/2 < r < 1$ of angle $\pi/2$ centered at a sidewall. The results are shown as instantaneous x-distributions in Fig. 3 and on the $x-t$-plane in Fig. 4. The data for two opposite sidewalls are indicated as 'east' and 'west'.

We have identified two types of flow regimes with turbulent spots. One type, illustrated in Figs. 2a,c, 3 and 4a,b, has been observed at higher Ha ($Ha \geq 20$ for pipe and $Ha \geq 23$ for duct), i.e. closer to laminarization. Its distinctive feature is that, apart from the rare dynamic events to be discussed shortly, each spot maintains its identity, approximately constant length $\sim 25 - 30$, and speed ~ 0.9 during the entire simulation, up to 2000 time units. The TKE distribution along a spot typically shows a maximum in the middle and decreases gradually towards the ends (see Fig. 3). The TKE of an isolated spot depends only on Ha decreasing from ~ 0.07 at lower Ha to ~ 0.05 at high Ha.

The length and energy of individual spots have been repeatedly reproduced in all our pipe and duct simulations. At the same time, the number of spots and the distance between them demonstrate non-uniqueness and strong sensitivity to initial conditions. For example, two regimes with spots localized at either one or both sidewalls (as in Fig. 2c) are obtained in two runs identical in all respects but the initial conditions, which are the turbulent states at $Ha = 0$ separated by 20 time units. Similarly, the flows in Fig. 3 are obtained in the same system but with different initial conditions: turbulent flow at $Ha = 20$ (Fig. 3a) or a two-spot flow at $Ha = 25$ computed in a shorter domain (Fig. 3b).

There is a clear analogy between our high-Ha turbulent spots and turbulent puffs in the HD pipe flow [22–26], except for some difference in the typical length (about 40 in the HD pipe). The term 'puff' is used in the following.

Rich dynamics of puffs has been found in our simulations. Some features are related to the sidewall localization and are completely unique. In particular, the puffs developing at the opposite walls tend to form staggered patterns (see Fig. 3). In the pipe flow, we have also observed events of 'locking', when the two puffs forming on the opposite sides travel together apparently locked by mutual perturbation (see Fig. 2a).

Other features have counterparts in HD systems. For example, we observed gradual merging of two puffs located at the same wall near each other (point `M` in Fig. 4b). Gradual stretching of a puff followed by its splitting into two puffs was also detected (points `S` in Figs. 4a,b). The splitting was often followed by a long phase of 'chaining', in which two new puffs traveled together separated by a short distance (Fig. 3b, west) or connected in a bi-maxima structure (Fig. 3b, east). In several cases, a sequence of stretching, splitting, chaining, and then merging was found.

The second kind of turbulent spots, which we call 'extended turbulent zones', has been observed at lower Ha ($Ha = 22$ for the duct and $Ha = 19$, 20 for the pipe) (Figs. 2b, 4c-d). These spots appeared only in some simulations, usually when a puff flow at a higher Ha was taken as an initial condition. In the other simulations, a rapid transition to a flow with two fully turbulent sidewall layers and laminar core occurred. Unlike puffs, the extended zones do not have typical length or energy. Turbulence is present over the entire length of the flow domain, either on both sides in the form of staggered structure (Figs. 2b) or on one side. The total TKE of the extended zone states is only slightly (5-10%) smaller than the TKE of the states with fully turbulent sidewall layers observed at the same Ha.

Some analogy can be traced between our extended zones and the intermittency structures obtained for HD pipe in computations with growing Re [24]. We have emulated [24] conducting duct simulations starting with puff regimes at $Ha = 25$ and decreasing Ha to 22. Flows at $L_x = 32\pi$ with a puff on one or two sides have been used as initial conditions. In the first case, long-time (hundreds of time units) evolution results in a quasi-stationary state with two-sided staggered extended zones (Figs. 2b, 4c). In the second case, the turbulence zone on one side spreads until it fills the entire duct length (Fig. 4d), while the other side and the core remain laminar.

The results reported so far are obtained using long computational domains: at least 80 for the pipe and 32π for the duct. We have also conducted simulations in shorter domains and found a strong effect. The range of Ha, in which the states with isolated turbulent spots are found, reduces with decreasing L_x. No puffs appear in domains shorter than 20. Instead, the transitional states have either one or two completely turbulent sidewall layers. Single puffs are found on one or two sides of pipes with $L_x = 40$ and ducts with $L_x = 16\pi$. We conclude that an accurate simulation of the transitional regimes at moderate Re and Ha requires a domain several times longer than a typical puff (at least ~ 80 half-widths or radii). The earlier results obtained in shorter domains [18, 19, 28, 29] have to be considered critically in this respect. A similar conclusion is suggested by the results of [30].

Our work has two major conclusions. First, the classical experiments [2], provide high quality results that stand the test by modern numerical analysis. Second, for the duct and pipe MHD flows, there exists a substantial area on the Re-Ha plane, where they are neither laminar nor turbulent, but have laminar cores and Hartmann layers as well as sidewall layers consisting of laminar zones and turbulent puff-like or extended turbulent spots. The behavior of these states does not differ significantly between the pipe and the duct. Our results also help to resolve the apparent inconsistency of the experimental data concerning the duct flow transition. Experiments at high Ha [10] show transition at $R = Re/Ha \sim 400$, while the experiments at moderate Ha indicate transition at $R \sim 200$ [2, 31]. Our results together with the recent high-Ha computations [17, 28] show that turbulence appears at $R \sim 200$, albeit only near the sidewalls. This is not registered in the high-Ha experiments because the total friction is dominated by the friction in the laminar Hartmann layers. Accordingly, the change in friction behavior caused by transition in isolated Hartmann layers at $R \sim 400$ [14] is found.

Our study leaves some unanswered questions about the turbulent spots. It is unclear whether their existence is limited to moderate Re or they can appear at higher Re and Ha. Our simulations at $Re = 10^5$, $Ha \leq 400$ [28] did not show them, but the domain length in [28] was just 4π. Other questions concern the nature of turbulent puffs, in particular, their lifetime statistics, dynamics of streamwise streaks and hairpin vortices, and the nature of the edge of chaos state. It would be interesting to extend the reaction-diffusion model for puffs in HD pipe flow [32] to the locking between puffs in MHD pipe flow.

There is another potentially interesting aspect that may make high-Ha flows an attractive system for studying dynamics of patterned turbulence. As the ratio of sidelayer width to its vertical size decreases with Ha, structures may appear that do not occupy the full vertical range in analogy with the turbulent bands in Couette flow [30]. Therefore, MHD pipe or duct flow can exhibit a continuous change from spots to bands controlled by increasing Ha.

Let us finally propose an experiment in the spirit of [2] that would significantly improve understanding of MHD flows. Up to now, all experiments have been carried out with liquid metals [2, 10, 11, 31], which do not permit flow visualization. Experiments using a transparent liquid such as saltwater and applying stereoscopic PIV could reveal the structure of the flow. Since the electric conductivity of electrolytes is four orders of magnitude lower than of liquid metals, higher magnetic fields would be necessary to achieve the same Ha. An experiment in a pipe or duct of width 0.1 m and length ~ 10 m requires a long uniform magnetic field ~ 1 T. Such a magnet system could be either created by superconducting coils or by rare-earth permanent magnets in the form of Halbach cylinders [33]. This makes electrolyte Hartmann experiments feasible in the future.

Financial support was provided by the Deutsche Forschungsgemeinschaft (grants Bo 1668/5 and GRK 1567) and by the U.S. NSF (grant CBET 0966557). Computer resources were provided by the computing centers of Forschungszentrum Jülich (NIC) and TU Ilmenau.

[1] J. Hartmann, K. Dan. Vidensk. Selsk. Mat. Fys. Medd. **15 (6)**, 1 (1937).

[2] J. Hartmann and F. Lazarus, K. Dan. Vidensk. Selsk. Mat. Fys. Medd. **15 (7)**, 1 (1937).

[3] H. K. Moffatt, *Magnetic field generation in electrically conducting fluids* (Cambridge Univ. Press, 1978).
[4] J. A. Shercliff, *The Theory of Electromagnetic Flow-measurement* (Cambridge University Press, 1962).
[5] F. Stefani, T. Gundrum, and G. Gerbeth, Phys. Rev. E **70**, 056306 (2004).
[6] A. Thess, E. V. Votyakov, and Y. Kolesnikov, Phys. Rev. Lett. **96**, 164501 (2006).
[7] P. A. Davidson, Annu. Rev. Fluid Mech. **31**, 273 (1999).
[8] S. Smolentsev, R. Moreau, L. Bühler, and C. Mistrangelo, Fusion Eng. Design **85**, 1196 (2010).
[9] O. Reynolds, Philos. T. R. Soc. A **174**, 935 (1883).
[10] P. Moresco and T. Alboussière, J. Fluid Mech. **504**, 167 (2004).
[11] H. Branover, *Magnetohydrodynamic Flow in Ducts* (John Wiley, New York, 1978).
[12] P. J. Schmid and D. S. Henningson, *Stability and Transition in Shear Flows* (Springer Verlag, 2001).
[13] B. Hof, A. Juel, and T. Mullin, Phys. Rev. Lett. **91**, 244502 (2003).
[14] D. S. Krasnov, E. Zienicke, O. Zikanov, T. Boeck, and A. Thess, J. Fluid Mech. **504**, 183 (2004).
[15] D. Krasnov, O. Zikanov, M. Rossi, and T. Boeck, J. Fluid Mech. **653**, 273 (2010).
[16] D. Krasnov, O. Zikanov, and T. Boeck, Comp. Fluids **50**, 46 (2011).
[17] Y. Zhao and O. Zikanov, J. Fluid Mech. **692**, 288 (2012).
[18] S. Satake, T. Kunugi, and S. Smolentsev, J. Turb. **3**, 27 (2002).
[19] R. Chaudhary, S. P. Vanka, and B. G. Thomas, Phys. Fluids **22**, 075102 (2010).
[20] D. Krasnov, O. Zikanov, J. Schumacher, and T. Boeck, Phys. Fluids **20**, 095105 (2008).
[21] T. Boeck, D. Krasnov, and E. Zienicke, J. Fluid Mech. **572**, 179 (2007).
[22] I. J. Wygnanski and F. H. Champagne, J. Fluid Mech. **59**, 281 (1973).
[23] B. Eckhardt, T. M. Schneider, B. Hof, and J. Westerweel, Ann. Rev. Fluid Mech. **39**, 447 (2007).
[24] D. Moxey and D. Barkley, PNAS **107**, 8091 (2010).
[25] B. Hof, A. de Lozar, D. Kuik, and J. Westerweel, Phys. Rev. Lett. **101**, 214501 (2008).
[26] K. Avila, D. Moxey, A. de Lozar, M. Avila, D. Barkley, and B. Hof, Science **333**, 192 (2011).
[27] Y. Duguet, P. Schlatter, D. Henningson, and B. Eckhardt, Phys. Rev. Lett. **108**, 044501 (2012).
[28] D. S. Krasnov, O. Zikanov, and T. Boeck, J. Fluid Mech. **704**, 421 (2012).
[29] V. Shatrov and G. Gerbeth, Phys. Fluids **22**, 084101 (2010).
[30] G. Brethouwer, Y. Duguet, and P. Schlatter, J. Fluid Mech. **704**, 137 (2012).
[31] W. Murgatroyd, Philos. Mag. **44**, 1348 (1953).
[32] D. Barkley, Physical Review E **84**, 016309 (2011).
[33] M. Abele, *Structures of permanent magnets: generation of uniform fields* (Wiley, 1993).